Comprehensive Landscape of Non-muscle Invasive Bladder Cancer Tumour Microenvironment and Prognostic value of Cancer-Associated Myofibroblasts

Carmen G. Cañizo[1], Félix Guerrero-Ramos[1], Mercedes Perez-Escavy[2, 3, 4], Iris Lodewijk[2, 3, 4], Cristian Suárez-Cabrera[2, 3, 4], Lucía Morales[2, 3, 4], Sandra P Nunes[2, 4, 5], Ester Munera-Maravilla[2, 3, 4], Carolina Rubio[2, 3, 4], Rebeca Sánchez[6, 7], Marta Rodriguez-Izquierdo[1], Jaime Martínez de Villarreal[3, 8], Francisco X. Real[3, 8, 9], Daniel Castellano[10], Cristina Martín-Arriscado[11], Alfredo Rodríguez Antolín[1], Marta Dueñas[2, 3, 4], Jesús M. Paramio[2, 3, 4 †], Victor G. Martínez[2, 3, 4 *]

[1]Urology Department, University Hospital '12 de Octubre', Madrid, Spain

[2]Molecular and Traslational Oncology Division, Biomedical Innovation Unit, CIEMAT, Madrid, Spain

[3]Centro de Investigación Biomédica en Red Cáncer (CIBERONC), Madrid, Spain.

[4]Institute of Biomedical Research, University Hospital '12 de Octubre', Madrid, Spain

[5]Cancer Biology and Epigenetics Group, Research Center of IPO Porto (CI-IPOP)/CI-IPOP@RISE (Health Research Network) Porto Comprehensive Cancer Center Raquel Seruca (Porto.CCC), Porto, Portugal.

[6]Cell Technology Division, Biomedical Innovation Unit, CIEMAT, Madrid, Spain

[7]Centro de Investigación Biomédica en Red Enfermedades Raras (CIBERER), Madrid, Spain

[8]Epithelial Carcinogenesis Group, Spanish National Cancer Centre-CNIO, Madrid, Spain

[9]Departament de Medicina i Ciències de la Vida, Universitat Pompeu Fabra, Barcelona, Spain

[10]Oncology Department, University Hospital '12 de Octubre', Madrid, Spain

[11]Scientific Support Unit, Research Institute I+12, University, Hospital 12 de Octubre Madrid, Spain.

* Lead contact and corresponding author

† Senior author

* **Correspondence**: Avenida Complutense 40, 28049 Madrid, Spain

Telephone number: 0034 687261559

victormanuel.garcia@externos.ciemat.es

Keywords: Cancer-associated fibroblasts; Myofibroblasts; Non-muscle invasive bladder cancer; Programmed death ligand-1; Tumour microenvironment

Word count of the text: 3717

Word count of the abstract: 299

ABSTRACT

Background: Non-muscle-invasive bladder cancer (NMIBC) is challenging due to high recurrence and progression rates. Bacillus Calmette-Guérin (BCG) is the standard treatment for high-risk NMIBC, but emergence of anti-PD-1/PD-L1 drugs necessitates a deeper understanding of the tumour microenvironment (TME) for improved prognostic markers and therapies.

Objective: To extensively analyse NMIBC's TME, focusing on cellular composition, PD-L1 expression, and the role of cancer-associated fibroblasts (CAFs) in prognosis.

Design, Setting, and Participants: A prospective study between December 2019 and December 2022 collected 98 NMIBC and non-pathological tissue (NPT) samples from cytology-positive/suspicious patients (66 patients in final analysis).

Intervention(s): Assessment of immune and non-immune cell subsets and PD-L1 expression using flow cytometry. Transcriptomic data and histology validated findings and evaluated prognostic markers.

Outcome Measurements and Statistical Analysis: We assessed the distribution of 11 cell types and PD-L1 expression in NMIBC, comparing them to NPT and across pathological stage and grade. Statistical methods evaluated the association of myofibroblasts (myoCAFs) and other CAF subsets with progression-free and recurrence-free survival.

Results and Limitations: Compared to NPT, NMIBC's TME exhibited microvascular alterations, increased fibroblast and myoCAF presence, and varying immune cell distribution. Heterogeneous PD-L1 expression was observed across subsets, with cancer

cells as primary potential anti-PD-L1 binding targets. MyoCAFs were associated with high grade tumours and poor prognosis, while other CAF subsets were not. Study limitations included a modest sample size and a relatively short follow-up period.

Conclusions: This comprehensive analysis provides a roadmap to establish the full NMIBC's TME, highlighting myoCAFs as potential prognostic markers. Understanding its complexity may enhance therapeutic strategies and risk stratification for NMIBC patients. Further research is essential to validate findings and explore myoCAF implications in NMIBC therapy.

Patient Summary: We described the composition of non-muscle invasive bladder cancer, identified cellular components associated with aggressive tumors, and found markers to predict outcome.

73 **INTRODUCTION (342)**

74 The tumour microenvironment (TME) varies among tumours, main elements including
75 immune cells, stromal cells, blood vessels and non-cellular components such as the
76 extracellular matrix [1]. While there is a wealth of works that study the TME in advanced
77 bladder cancer (BLCA) [2–6], this topic has been neglected in non-muscle invasive BLCA
78 (NMIBC), specially for the non-immune TME. TME components can impact on therapy
79 response, as has been shown for many solid tumours, including advanced BLCA. Hence,
80 a better characterisation of the TME in NMIBC is important in order to fully understand
81 the biology of these tumours and to improve their management.

82 The use of anti-programmed death ligand-1 (PD-L1) check point inhibitors is rising as a
83 novel treatment in high risk NMIBC due to limited efficacy of Bacillus Calmette-Guérin
84 (BCG) therapy [7], where up to 50-70% of BCG-treated patients will experience a high-
85 grade recurrence despite the instillations [8]. Despite promising preliminary results, the
86 response to these drugs varies among patients [9,10]. A deeper insight of the molecules
87 targeted by these immunotherapies is pivotal to identify which patients might respond
88 to them. While assessment of PD-L1 expression is valuable for patient stratification in
89 certain cancers, its usefulness in BLCA is a matter of debate, especially in NMIBC.
90 Besides, not only tumour cells but other TME subsets express PD-L1, which may impact
91 on therapy response and prognosis.

92 We hypothesized that a better characterisation of the TME composition and PD-L1
93 expression in NMIBC may help understanding the tumour biology and find new
94 prognostic biomarkers and targets. This work is a prospective study in which tumour and
95 non-pathological tissue from 66 NMIBC patients were analysed. While presence of T cell

96 subtypes are well characterised in NMIBC, we focused on less studied myeloid and non-
97 immune populations. Here, we provide a reference map of the frequencies of 11 cell
98 subsets in NMIBC and quantified accurately PD-L1 expression in all cell populations.
99 Utilizing computational tools we found that aSMA-expressing cancer-associated
100 fibroblasts (myoCAFs) serve as prognostic biomarkers in these patients, and validated
101 these findings with different techniques and patient cohorts.

102

103

MATERIALS (PATIENTS) AND METHODS (811)

Patients and samples

We recruited 98 patients with BLCA diagnosis between December 2019 and December 2022 at an academic tertiary referral hospital. Patients with muscle-invasive bladder cancer (MIBC), carcinoma in situ and those from whom we could not obtain an acceptable sample were excluded. The study was enriched for high grade, high risk tumours based on the greater clinical need for this patient population. Clinical and demographic data are summarized in supplementary table 1. This study was approved by Research Ethics Committee of the University Hospital “12 de Octubre” and informed consent was obtained from all patients.

Tissue processing

Biopsies were carefully cut into small pieces and digested to obtain single cell suspensions (supplementary methods). Then, cells were stained with Zombie aqua (BioLegend) and used for immunofluorescence staining [11]. All antibodies and kits used can be found in supplementary table 2. Samples were run in a LRSFortessa X20 flow cytometer (BD Biosciences) and analysed using the FlowJo software (FlowJo, LLC) and OMIQ platform. Computational analysis of flow cytometry data can be found in supplementary methods.

IHC and immunofluorescence

Nineteen FFPE BLCA sections (7 G1, 9 G2 and 2 G3) were stained with antibodies against aSMA, CD163, PanCK and DAPI. Antigen retrieval was performed using a pressure cooker (Dako, Agilent Technologies). Primary antibodies were incubated overnight. Antibodies

126 used are shown in supplementary table 2. The IHC signal was amplified with a biotin-
127 avidin-peroxidase system (ABC Elite Kit Vector) and visualized using diaminobenzidine
128 (DAB Kit, Vector Laboratories). For immunofluorescence, 4',6-diamidino-2-phenylindole
129 (DAPI) was used to stain nuclei and images were taken with a Zeiss Axioimager 2
130 fluorescence microscope. Cytometry analysis of immunofluorescent tissue sections can
131 be found in supplementary methods.

132 **Single cell RNA-seq analysis**

133 Single cell data from Chen et al. was analysed from raw fastq data. Briefly, reads were
134 pseudoaligned to GRCh38 cDNA sequence assembly using 'kallisto bus' command
135 (Kallisto software, default parameters) and sparse matrices were generated bustools
136 program and BUSspaRse R package as described [12]. Individual sample matrices loaded
137 with Seurat package were merged in a common object. Data was normalized
138 (sctransform and log normalization for the top 2000 variable genes) and stored as two
139 different slots of the same Seurat object. Linear dimensionality reduction was
140 performed using the first 20 principal components (PC) according to elbow plot
141 visualization. Non-linear dimensional reduction (UMAP) and clustering were performed
142 using these PCs. Cluster stability was visualized in a clustree analysis (resolution set to
143 0.2). FindAllMarkers was used for cell annotation. Macrophages were extracted and
144 reanalysed as an independent object. Functional analysis was performed using VISION
145 R package [13] and the resulting signature scores were incorporated as metadata to the
146 Seurat object. Construction of gene-signature scores was done using 2 and 4-fold change
147 differentially expressed genes for each subset or by previously published gene sets, all

148 shown in supplementary table 3. Scores were calculated by averaging gene expression
149 z-scores within a signature.

150 **Tissue microarray**

151 Cores from formalin-fix paraffin embedded tissue blocks were used to construct tissue
152 microarrays (TMA; 1.5-mm core diameter), with at least two duplicate cores per case (n
153 = 29), using a standard manual method (Beecher Instruments) [14]. TMAs were stained
154 with H&E and sections were reviewed to confirm the presence of representative tumour
155 tissue. Demographic, clinical and pathological data is summarised in supplementary
156 table 4.

157 **Statistical Analysis**

158 Categorical variables were expressed as absolute and relative frequency. Continuous
159 variables were expressed as median (interquartile range; IQR) according to a normality
160 test (Kolmogorov–Smirnov test). Comparisons were performed using the Wilcoxon–
161 Mann–Whitney test (for two groups) or the Kruskal–Wallis test (for more than two
162 groups) with Dunn´s multiple comparison test. The Spearman correlation analysis
163 method was used to determine the correlation strength and direction between
164 variables.

165 The survival analyses were performed using the Kaplan–Meier method and described by
166 median and range. Differences between groups were tested using the log-rank test. A
167 Cox proportional hazards model was fitted to estimate hazard ratio (HR) and the
168 corresponding 95% confidence interval (CI). A multivariable model was created with all
169 confounding and relevant factors and had a p-value of <0.1 in the univariate analysis.
170 The best multivariable statistical model was selected using Akaike Information Criterion.

171 A logistic regression model was created to evaluate the risk factors associated with
172 tumor grade. The study was completed with a multivariable analysis. A step-by-step
173 selection process was used to highlight the most relevant factors, to identify the
174 significant sets among variables and to avoid confusion in the model. We used odds
175 ratios (ORs) and 95% confidence intervals (CIs) to present the results of the regression
176 analysis.

177 All analyses were done using Stata InterCooled for Windows version 16 (StataCorp.
178 2019. Stata Statistical Software Release 16, StataCorp LLC, College Station, TX, USA),
179 GraphPad Prism version 9 for Windows (GraphPad Software, Boston, Massachusetts
180 USA) and R (version 4.2.1; R Foundation for Statistical Computing, Vienna, Austria) and
181 a level of significance of 5%.

182 **Data Sharing Policy**

183 Data are available for bona fide researchers who request it from the authors.

184

185 **RESULTS (1333)**

186 **Clinical and pathological information**

187 We prospectively collected and processed 98 fresh tumour and non-pathological tissue
188 (NPT) samples according to the schematic in figure 1A. After quality control, we included
189 66 NMIBC tumour samples and 62 NPT biopsies in the final analysis (84.4% matched
190 tumour-NPT ratio). Among the 66 tumours, 27 were T1 and 39 were Ta, with grade
191 classifications of 15 grade 1, 18 grade 2, and 33 grade 3 (68% high risk). Supplementary
192 Table 1 offers a detailed summary of clinical and histopathological information.

193 **Tumour microenvironment landscape of NMIBC**

194 We designed two multicolour panels for immune and non-immune subset detection,
195 including PD-L1 expression, which allowed identification of 11 cell types (figure 1A).
196 Gating strategy described in supplementary figure 1A-B. Relative proportions varied
197 widely between NPT and tumours (figure 1B). NPT samples had abundant T cells (28.26
198 ± 15.17%). Tumours primarily had cancer cells (44.1 ± 29.5%) followed by T cells (19.11
199 ± 16.96%). Stromal cells, T cells, NK cells, and cDC2 were all decreased in tumors, while
200 macrophages were increased, in accordance to literature. To mitigate the impact of the
201 urothelial cell content in tumour samples, we examined cellular compartments (figure
202 1C). TME showed increased endothelial cells, suggesting angiogenesis. All non-immune
203 stroma subsets differed significantly between NPT and tumours. The immune
204 compartment changes paralleled those from whole tissue results, indicating differential
205 recruitment in tumours. We found also fibroblast activation and M2-like differentiation
206 of macrophages increased in tumours (supplementary figure 1C). These results suggest
207 overall cancer-associated inflammation in NMIBC, as expected.

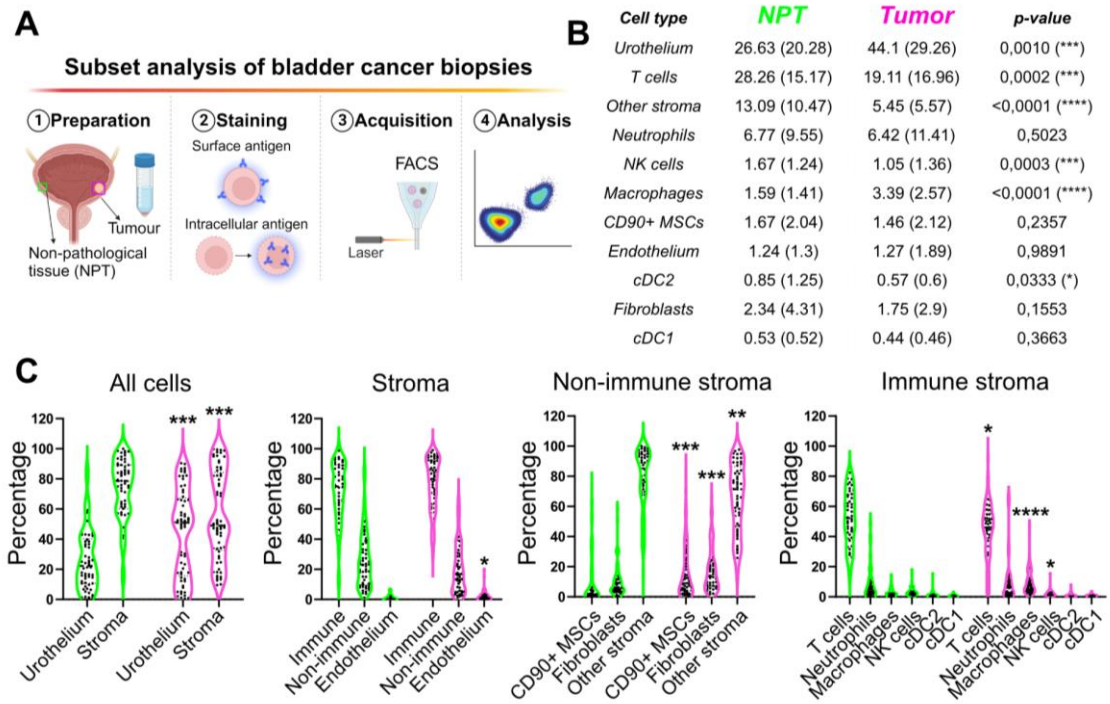

Cell type	NPT	Tumor	p-value
Urothelium	26.63 (20.28)	44.1 (29.26)	0,0010 (***)
T cells	28.26 (15.17)	19.11 (16.96)	0,0002 (***)
Other stroma	13.09 (10.47)	5.45 (5.57)	<0,0001 (****)
Neutrophils	6.77 (9.55)	6.42 (11.41)	0,5023
NK cells	1.67 (1.24)	1.05 (1.36)	0,0003 (***)
Macrophages	1.59 (1.41)	3.39 (2.57)	<0,0001 (****)
CD90+ MSCs	1.67 (2.04)	1.46 (2.12)	0,2357
Endothelium	1.24 (1.3)	1.27 (1.89)	0,9891
cDC2	0.85 (1.25)	0.57 (0.6)	0,0333 (*)
Fibroblasts	2.34 (4.31)	1.75 (2.9)	0,1553
cDC1	0.53 (0.52)	0.44 (0.46)	0,3663

Figure 1. Analysis of cell subset frequencies from total and cellular compartments. A) Schematic representation of the prospective study design. Non-pathological and tumour tissue biopsies were collected and digested to obtain single cell suspensions. Samples were then stained for surface and intracellular markers and analysed in a flow cytometer. B) Frequencies for the indicated cell lines were determined for 62 NPT and 66 tumour samples. Mean and standard deviation (in brackets) of the frequencies from total cells for each cell subset is shown. C) Frequencies of cell subsets within the corresponding cell compartment. Each dot represents one patient data. Statistical analysis in B and C was done by Wilcoxon–Mann–Whitney test. * p-value<0.05; ** p-value<0.005; *** p-value<0.0005;**** p-value<0.0001. MSC= mesenchymal stromal cells; NK cells=natural killer cells; cDC=conventional dendritic cells.

221 To analyse how the NMIBC TME changes as tumour progresses, we analysed pT2G3
222 tumours (n=8) (supplementary figure 2). Stromal infiltration increased from pTa to pT2,
223 but leukocyte enrichment remained unchanged (supplementary figure 2A-B and D-E).
224 Only Mesenchymal Stromal Cells (MSCs) and Natural Killer (NK) cells showed significant
225 association to pT stage (supplementary figure 2C). Regarding tumour grade, cDC2 were
226 decreased, while MSCs and fibroblasts increased in G3 tumours (supplementary figure
227 2F). Our results reveal that despite the lack of muscle invasion, NMIBC tumours, present
228 a diverse microenvironment with prominent recruitment of structural and myeloid cells.

229

230 **Increased PD-L1 expression in NMIBC comes from the TME**

231 Anti-PD-L1 therapies have emerged for NMIBC management, prompting PD-L1
232 expression assessment in tumour compartments. NMIBC presented elevated bulk PD-
233 L1+ cells vs. NPT (figure 2A & B, upper panels). Notably, PD-L1+ cell increase in tumours
234 stemmed mainly from infiltrate, while cancer cells showed similar PD-L1 to urothelium
235 (figure 2A & B). Subset analysis shows that macrophages had the most PD-L1+ cells, with
236 anti-inflammatory M2-like macrophages especially rich in PD-L1 (figure 2C). cDC2 and
237 tumour cells followed, the later averaging 20% (± 14.42) PD-L1+ cells, along with non-
238 immune stromal cells. Of note, aSMA-expressing fibroblasts had higher proportion of
239 PD-L1+ cells than total fibroblasts. NK and T cells had lower PD-L1 levels as expected.
240 Next, we sought to highlight key anti-PD-L1 treatment potential binding targets in
241 NMIBC. We gated out total PD-L1+ cells and then applied our previous gating
242 (supplementary figure 1A and B). Cancer cells emerged as the primary binding target,
243 constituting 60% of PD-L1+ cells, surpassing macrophages and aSMA+ fibroblasts which

244 showed high proportion of PD-L1+ cells (figure 2D). Notably, cells with less understood
245 PD-L1 function like Neutrophils and T cells accounted together for a relevant 10% of anti-
246 PD-L1 targets. This underscores the need for further investigating PD-L1's role in TME
247 subsets. While we quantified PD-L1+ cell dynamics with tumour progression in major
248 compartments, no significant correlations emerged between cancer stage or grade and
249 PD-L1+ cell proportions (supplementary figure 3).

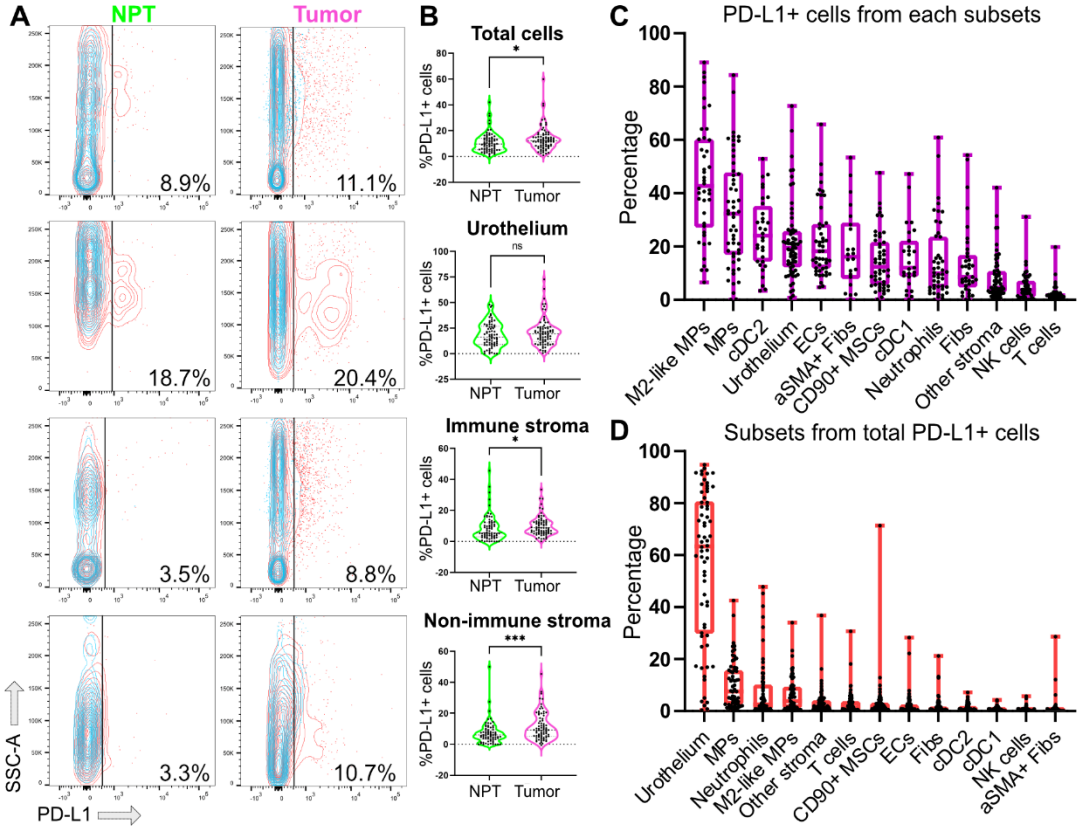

250

251 **Figure 2. Heterogeneous expression of PD-L1 in cancer and TME cells in NMIBC**. A-B)
252 Percentage of PD-L1+ cells was calculated using fluorescent minus one controls (blue
253 overlay) for all cells and main cellular compartments, and representative examples (A)
254 and dispersion plots (B) are shown. Each dot represents one patient data. Comparisons
255 were done by Wilcoxon–Mann–Whitney test. * p-value<0.05; *** p-value<0.0005; ns
256 non-significant. SSC-A= scatter signal channel area. NPT, non-pathological tissue. C) Box

257 plots showing percentage of PD-L1 positive cells within the indicated cell subsets. Each
258 dot represents one different patient. Median and interquartiles are shown. Subsets are
259 ordered from higher median of PD-L1+ cells to lowest. D) PD-L1 positive cells were gated
260 from total cells and subset analysis was run in this set of cells. Each dot represents one
261 different patient. Median and interquartiles are shown. Subsets are ordered from higher
262 to lower frequency median. MP = macrophages; cDC = conventional dendritic cells; ECs
263 = endothelial cells; Fibs = fibroblasts; MSCs = mesenchymal stromal cells.

264

265 **M2-like macrophages and myofibroblasts are associated to high grade NMIBC**

266 We used our flow cytometry data to identify markers linked to aggressive NMIBC.
267 Employing computational tools in an agnostic approach, we first fine-tuned our method
268 by comparing NPT and tumour samples, verifying findings which paralleled the manual
269 gating (supplementary figure 1 and 4). Subsequently, we focused on tumour samples
270 and generated optimized clustering in both datasets (figure 3A and F), revealing multiple
271 high-grade enriched cell clusters. In the myeloid panel, cluster k7-5 exhibited
272 macrophage markers and variable M2-like-associated markers (figure 3B-D). Manual
273 gating confirmed the enrichment of total macrophages and M2-like macrophages in
274 high-grade NMIBC, aligning with prior research [11]. For the stromal/lymphoid dataset,
275 two high-grade enriched clusters emerged, although only one could be defined with the
276 available information (figure 3G-I). Cluster k15-04 presented high CD90 and podoplanin
277 expression, hence being designated as cancer-associated fibroblasts (CAFs), and showed
278 expression of aSMA. Manual gating confirmed the association of total and aSMA+
279 fibroblasts with high-grade NMIBC (figure 3E and J). In summary, our unbiased analysis

pinpointed two cell types with distinct functional phenotypes enriched in high-grade NMIBC, holding promise as potential cellular prognostic biomarkers.

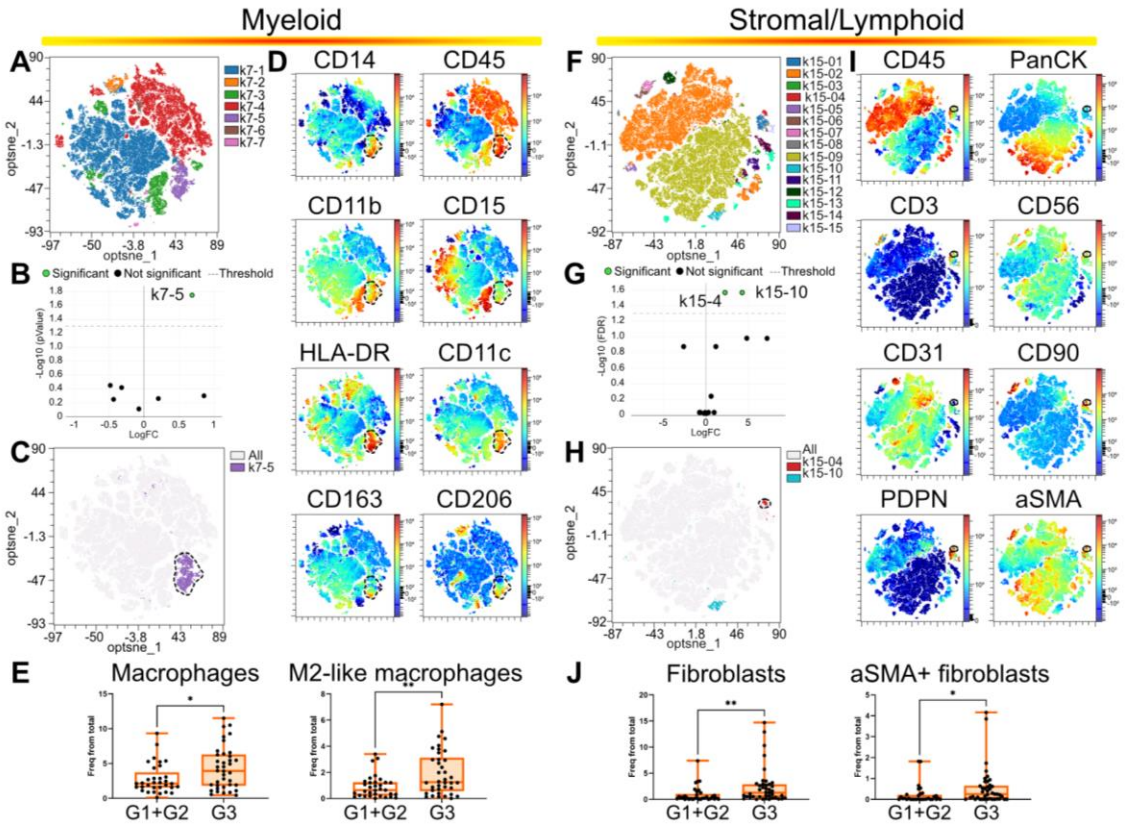

Figure 3. Total and specific macrophage and fibroblast subsets are enriched in high grade NMIBC. Computational analysis of flow cytometry data from the myeloid panel (A-E) and stromal/lymphoid panel (F-J). (A and F) Dimensions reduction was done using optSNE and semi-supervised clustering by FlowSOM setting at 7 and 15 the number of metaclusters for the myeloid and stromal/lymphoid panel respectively. (B, G) G1/G2 versus G3 comparison was done by EdgeR method to determined clusters underrepresented/enriched in G3 tumours. (C, H) Differentially represented cell clusters are shown in the optSNE maps. (D, I) Color-coded optSNE maps show the expression of the indicated markers. Dotted lines highlight differentially represented clusters. (E, J) Results from manual gating validation for the indicated cell subsets. Each dot represents

293 one different patient. Median and interquartiles are shown. Statistical analysis was done
294 by Wilcoxon–Mann–Whitney test. * p-value<0.05; ** p-value<0.005.

295

296 **M2-like macrophages and myoCAF crosstalk changes with tumour progression**

297 Reports show macrophage-fibroblast crosstalk in solid tumours, but it is unexplored in
298 NMIBC. We observed a positive correlation between M2-like macrophages and
299 fibroblasts in NMIBC (figure 4A), suggesting crosstalk. However, this correlation
300 decreased in high-grade tumours (figure 4B). To investigate this, we used aSMA and
301 CD163 as markers for CAFs and M2-like macrophages, respectively, in tumour sections.
302 Image quantification hinted at more CAFs in G3 tumours, while we could not confirm
303 higher percentage of CD163+ macrophages (figure 4C). Analysing their spatial
304 relationship, CD163+ macrophages were farther from CAFs in G1 tumours (figure 4D and
305 E). This changed drastically in G2 tumours with closer proximity, while G3 tumours
306 presented increased separation, indicating evolving microenvironment dynamics.

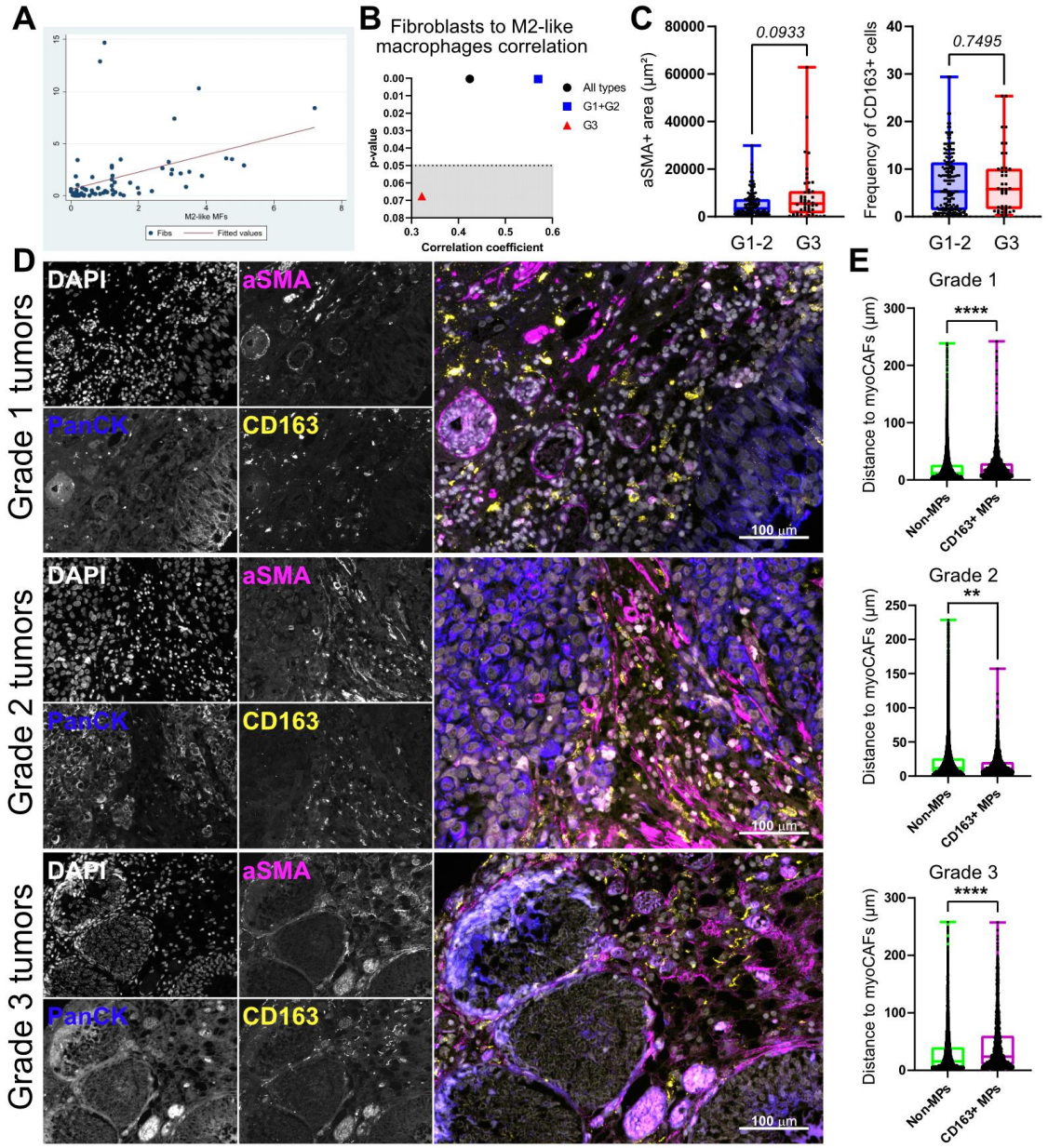

Figure 4. Fibroblast-macrophage interactions decrease in high-grade NMIBC. A) Correlation plot of M2-like macrophage and fibroblast frequencies from total cells in all NMIBC samples analysed. B) p-value against correlation coefficient in all samples and G1-2 and G3 groups. Dotted line marks statistical significance for data points above (grey area non-significant). C-E) FFPE tissue sections were stained for Cytokeratins (PanCK), M2-like macrophages (CD163) and myoCAFs (aSMA), plus DAPI to stain nuclei. Using the Qupath software, cytometric analysis was applied to determine the area of aSMA

315 staining, excluding the vasculature, and percentage of CD163 positive cells (C). D)
316 Representative examples for grade 1, 2 and 3 tumour stainings. E) Quantification of the
317 minimum distance to non-vasculature aSMA+ areas for all CD163-negative (non-MPs)
318 and CD163-positive (CD163+ MPs) cells. P-values and significance (asterisks) by
319 Wilcoxon–Mann–Whitney test are shown. ** p-value<0.005; **** p-value<0.0001.

320

321 **Macrophage subset gene signatures fail to predict NMIBC prognosis**

322 To predict patient prognosis, and given short follow-up periods of our prospective
323 cohort, we explored transcriptomic data from NMIBC patients. Using a single-cell RNA-
324 seq dataset [5], we identified 8 macrophage clusters, with clusters 1, 2, and 3 showing M2
325 marker expression and resembling our flow cytometry data (supplementary figure 5A-
326 B). These clusters also exhibited high scores for immunosuppressive TAM subsets [15]
327 (supplementary figure 5C). We generated gene signatures for all relevant TAM subsets
328 (supplementary table 3) and challenged one of the largest NMIBC patient cohorts [16]. We
329 found a significant association between TAM cluster 2 and progression-free survival, but
330 all the other comparisons failed to predict prognosis (supplementary figure 5D-E). Thus,
331 immune suppressive macrophage subsets may not be a significant prognostic factor in
332 NMIBC.

333 **MyoCAFs serve as cellular predictors of bad prognosis in NMIBC**

334 We also assessed the patient cohort with gene signatures for total fibroblasts (panCAFs),
335 inflammatory CAFs (iCAFs), and myofibroblasts (myoCAFs), described in various solid
336 tumours [3]. PanCAFs and iCAFs showed no prognostic value in NMIBC patients for
337 recurrence-free (RFS) and progression (to MIBC)-free survival (PFS), confirmed with a

338 well-established panCAFs signature (supplementary figure 6A-B). Conversely, the
339 myoCAF signature associated with worse PFS and RFS, with statistical significance for
340 the latter (figure 5A). We confirmed this association using an alternative myoCAF
341 signature, resulting in this case in statistical association with both PFS and RFS
342 (supplementary figure 6C). We validated this association in an independent cohort,
343 highlighting a robust link between myoCAFs and RFS (figure 5A). Furthermore, myoCAFs
344 were enriched in the most aggressive UROMOL transcriptomic classes 2a and 2b
345 tumours (figure 5B), whereas panCAFs and iCAFs mainly associated with class 2b
346 tumours (supplementary figure 6D). Additionally, myoCAFs were enriched in genomic
347 classes 2 and 3 (figure 5C), linked to poorer RFS, unlike panCAFs and iCAFs
348 (supplementary figure 6E).

349

350

351

352

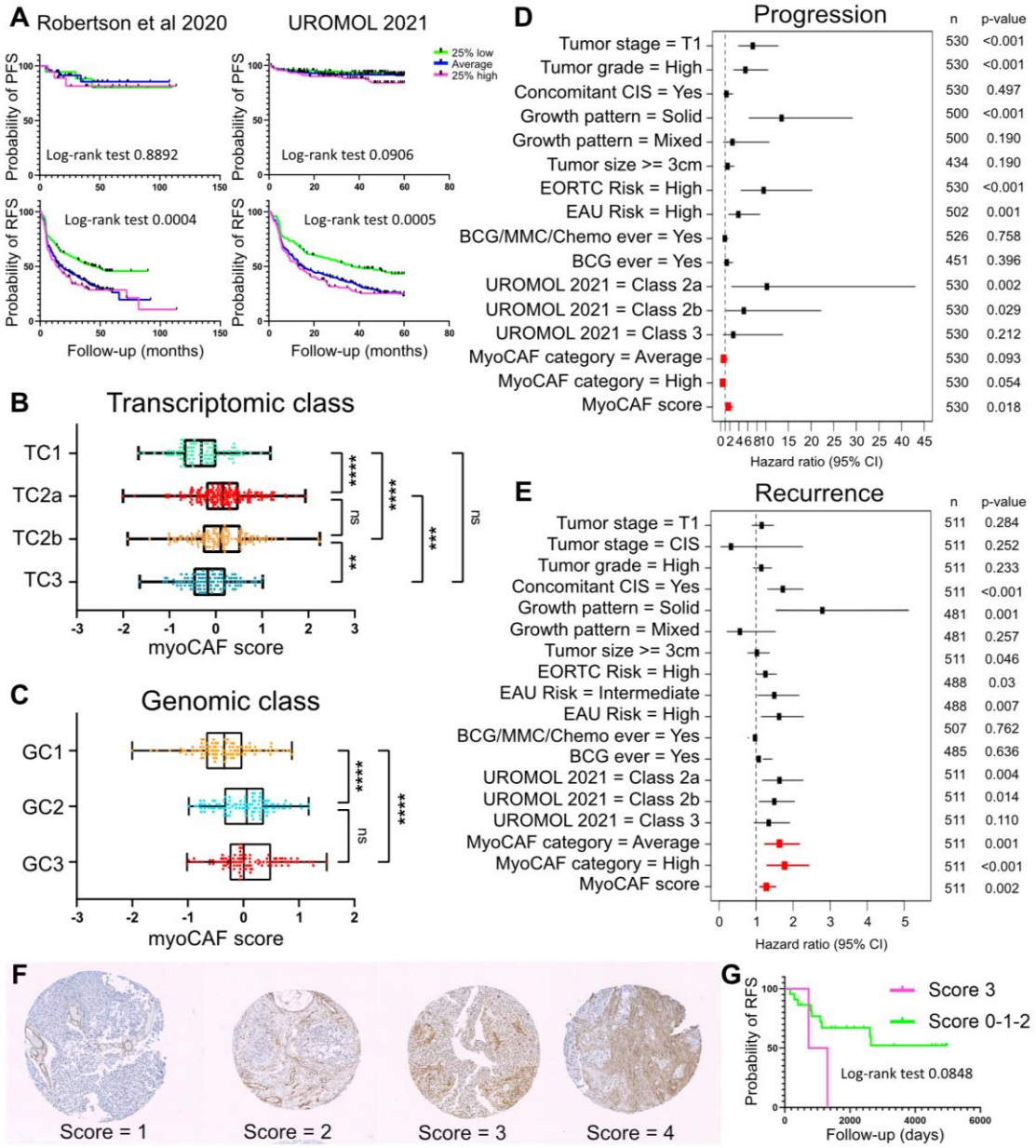

353

354 **Figure 5. Abundance of myoCAFs associates with bad prognosis in NMIBC.** A) A gene
355 signature score was generated for myoCAFs to challenge two independent
356 transcriptomic data cohorts of NMIBC. Patients were ranked according to this score and
357 three groups were formed. Kaplan–Meier plots for probability of progression-free
358 survival (PFS, upper panel) and recurrence-free survival (RFS, lower panels) for the two
359 cohorts are shown. Log-rank (Mantel-Cox) test was used to calculate statistical
360 significance between curves. B-C) Dotplox showing myoCAF scores for patients grouped

361 according to UROMOL 2021 transcriptomic classes (B) and genomic classes (C). Each dot
362 represents one patient. P-values ** < 0.005; *** < 0.0005; **** < 0.0001 Statistical
363 analysis was done with Kruskal-Wallis test with Dunn´s correction for multiple
364 comparisons. D-E) Overview of hazard ratios calculated from univariate Cox regressions
365 of progression-free (D) and recurrence-free (E) survival using clinical and molecular
366 features. Dots indicate hazard ratios and horizontal lines show 95% confidence intervals
367 (CI). P-values and sample sizes, n, used to derive statistics are indicated. CIS= carcinoma
368 in situ, EORTC= European Organisation for Research and Treatment of Cancer, EAU=
369 European Association of Urology. F) Representative immunohistochemistry images
370 showing aSMA expression in primary tumour sections from NMIBC patients. Histological
371 analyses and staining was performed in a TMA with duplicates for each tumour (n = 29).
372 All sections were scored from 0 to 3 according to aSMA staining density in non-
373 vasculature areas, to exclude pericytes. G) Kaplan–Meier plot for recurrence-free
374 survival in patients stratified by aSMA staining score. Log-rank (Mantel-Cox) test was
375 used to calculate statistical significance between curves.

376

377 Univariate Cox regression identified the myoCAF score as predictor of PFS (figure 5D).
378 Conversely, both myoCAF category and score strongly predicted RFS in NMIBC (figure
379 5E), with similar results in an independent cohort (supplementary figure 6F). Receiver
380 operating characteristic (ROC) analysis for progression prediction using logistic
381 regression models demonstrated a modest increase in accuracy when combining the
382 EAU risk score with concomitant CIS, growth pattern, and myoCAF category
383 (supplementary figure 6G). Similarly, combining the EAU risk score, transcriptional class

384 2a, and myoCAF score improved recurrence prediction (test of homogeneity p=0.0397),
385 from 0.532 to 0.576 (supplementary figure 6G). TMA using aSMA staining for myoCAFs
386 revealed a trend towards lower recurrence-free survival in patients with high myoCAF
387 staining (Log-rank test p-value = 0.0848) (figure 5G). Overall, these findings support
388 myoCAFs as potential biomarkers of recurrence in transcriptomic-based NMIBC
389 datasets.

390

391

392 **DISCUSION (828)**

393 Several studies have aimed at characterising the TME of NMIBC, with most
394 investigations making use of transcriptomic-based methods [16–20]. While very informative
395 intra-study, this type of analysis provides scores that are difficult to compare between
396 studies and are not well-suited in clinical practice. Immunohistological staining offers
397 comparative quantification of cell types, in addition to relevant spatial information, but
398 is limited by the number of markers that can be analysed simultaneously. Therefore,
399 most studies have focused on specific cell types, finding associations to therapy
400 response and prognosis, but failing to provide a wider picture of the NMIBC TME
401 landscape [21–23]. Our study is first to provide a reference map of relative proportions of
402 11 cell types. Comparison with non-pathological tissue allowed us to show cancer-
403 associated changes in the bladder mucosae. The compartment analysis provides a clear
404 picture of non-previously shown changes in NMIBC affecting the microvasculature, as
405 well as increased fibroblasts and MSC within the non-immune stroma. The differences
406 in the leukocyte compartment are in line with previous publications, with lower
407 presence of T cells but higher of macrophages and NK cells in tumours, which is further
408 exacerbated in MIBC [20,24] and supplementary figure 2C. This suggests a tumor promoting
409 role for these cells, as indicated in therapy response studies [22,25,26].

410 Immune checkpoint inhibitors targeting the PD-1/PD-L1 pathway have shown benefits
411 in MIBC, constituting a promising new treatment strategy in BCG-unresponsive high-
412 grade (HG) NMIBC and are under investigation in BCG naïve HG-NMIBC. Despite these
413 therapeutic results, the use of these targets as prognosis and predictive biomarkers is
414 much more controversial. Some studies have shown a significant association of high PD-

415 L1 expression to bad prognosis [27,28], to good prognosis [18,29–31], or no association [21,32–34].
416 Lack of concordance among techniques is unlikely to cause these discrepancies [35].
417 Nonetheless, most studies measure PD-L1 expression in the whole tissue section and/or
418 separating only tumour and immune-infiltrating cells, lacking the required biological
419 resolution. Our results show broad heterogeneity of PD-L1 expression among TME
420 subsets, suggesting most studies lack the granularity required to properly assess value
421 as a good prognosis biomarker. Furthermore, we demonstrate that, while relevant TME
422 cells express important levels of PD-L1, relative cellular abundancy suggests cancer cells
423 may act as a sink for anti-PD-L1 drugs. In addition, as opposed to other cancers [36], PD-L1
424 expression in NMIBC cells is similar to healthy urothelium. This suggests that immune
425 evasion via this molecule is a late event in BLCA progression.

426 CAFs have shown mostly a protumorogenic role in BLCA [37], although resident fibroblasts
427 have been shown to restrain tumour development in the early phases in a carcinogen-
428 induced mouse model [38]. These evidences suggest a switch in function as fibroblasts
429 differentiate into CAFs. Most studies addressing CAFs in BLCA have focused only on
430 MIBC or mixed cohorts, leaving NMIBC CAFs broadly ignored. We show here that
431 fibroblasts populate NMIBC, especially in high-grade tumours, with no differences
432 between Ta and T1 (data not shown). These results evidence that fibroblast recruitment
433 depend on cancer cell biology rather that level of invasion. Using different approaches,
434 we found that myoCAFs, but no other CAF subset, associate with bad prognosis in NMIBC
435 patients, as has been reported in MIBC [39,40]. Using immunohistochemistry, Mezheyeuski
436 et al tested CAF-associated markers in BLCA finding they also associated with HG-NMIBC
437 [41]. They found fibroblast activation protein (FAP) as the best predictor of poor outcome
438 although not when separating Ta, T1 and T2-4. Interestingly, aSMA was not statistically

439 associated to worse prognosis in the full cohort but it was for T1 tumours, in accordance
440 with our findings. In addition, a different CAF subset, named irCAFs, have been described
441 in a mix cohort of MIBC and NMIBC patients. irCAFs associate with worse overall survival
442 and neoadjuvant and immunotherapy response, including NMIBC, likely through
443 promotion of cancer stemness [3]. Future studies should apply more discriminatory
444 panels, and resolve the spatial distribution of cell types, to better characterise CAF
445 subsets in NMIBC.

446 We also found that CAF-macrophage crosstalk may change over NMIBC progression.
447 Increased interactions in early phases may correlate with co-attraction of both subsets
448 by BLCA cells via CXCL1 [42] and feedback loops via CCL2 and GM-CSF production by CAFs
449 [43]. According to our data, myoCAF-Macrophage crosstalk is reduced in high-grade
450 NMIBC, but this interaction is recovered in MIBC as described by others. These
451 observations likely reflect the dynamic nature of the TME as BLCA progresses, likely
452 influenced by cancer cell intrinsic characteristics plus evolution of the inflammatory
453 milieu since it appears tied to tumour grade progression.

454 Our results support a detrimental role of myoCAFs in NMIBC. Other authors have
455 proposed that bladder CAFs can promote BLCA growth via various factors [44–46], including
456 TGFβ [47–49], a key factor in myoCAF phisiology [50]. We show here that CAFs express PD-L1
457 and that this expression is increased in the myoCAF subset. It would be interesting to
458 measure expression on PD-L1 in other settings where PD-1/PD-L1 inhibitors are being
459 tested, such as BCG-unresponsive patients.

460

461 **CONCLUSIONS (67)**

462 The NMIBC TME is composed by a heterogeneous distribution of cancer, immune and
463 non-immune cells. These cell types exhibit differential features, such as PD-L1
464 expression, which study may contribute to improve patient management. Our results
465 strongly suggest that myoCAFs play an important role in NMIBC. Future studies, should
466 elucidate how and why myoCAFs associate with worse prognosis in order to find
467 appropriate targets to modulate their function.

468

469 **TAKE HOME MESSAGE (37)**

470 - The tumour microenvironment of NMIBC is rich in immune and non-immune
471 cells, with PD-L1 expression spread across multiple cell types.
472 - Cancer-associated fibroblasts (CAFs) and macrophages are enriched in high-
473 grade NMIBC.
474 - MyoCAFs predict bad prognosis in NMIBC patients.

475

476 **Acknowledgments**

477 We thank the Histology Laboratory from CIEMAT, namely Pilar Hernandez Lorenzo, for
478 the histological processing of tumour samples and the Laboratory of Cytometry and
479 Cellular Separation, specifically Omaira Alberquilla for their help with the flow cytometry
480 protocols and analyses. We acknowledge Miriam Marques, from the Epithelial
481 Carcinogenesis Group, Spanish National Cancer Centre-CNIO (Madrid) for critical
482 support in manuscript preparation. We acknowledge the following funding bodies:

NCT04134000 clinical trial, funded by Hoffmann-La Roche: Conduct of the study; collection, management of the data.

Grant SAF2015-66015-R and PID2019-110758RB-I00, funded by MCIN/AEI/ 10.13039/501100011033: design and conduct of the study; collection, management, analysis, and interpretation of the data; and preparation, review, or approval of the manuscript

Grant CIBERONC number CB16/12/00228, funded by Instituto de Salud Carlos III: Design and conduct of the study; collection, management, analysis, and interpretation of the data; and preparation, review, or approval of the manuscript.

V.G.M. supported by fellowships 2018-T2/BMD-10342 funded by Consejería de educación, universidades, ciencia y portavocia de la Comunidad de Madrid, INVES222946GARC funded by Fundación Científica de la Asociación Española Contra el Cáncer: Design and conduct of the study; collection, management, analysis, and interpretation of the data; and preparation, review, or approval of the manuscript.

S.P.N. supported by fellowship SFRH/BD/ 144241/2019) funded by FCT-Fundação para a Ciência e Tecnologia: Conduct of the study; Collection of data; review of the manuscript.

I.L. is supported by a predoctoral fellowship PRDMA19024LODE, funded by Fundación Científica de la Asociación Española Contra el Cáncer: Conduct of the study; Collection of data; review of the manuscript.

L.M. supported by fellowship POSTD19036MORA, funded by Fundación Científica de la Asociación Española Contra el Cáncer: Conduct of the study; Collection of data; review of the manuscript.

Declaration of Generative AI and AI-assisted technologies in the writing process?

During the preparation of this work the author(s) used ChatGPT in order to generate the abstract and assist in reducing the word count in section “MATERIALS (PATIENTS) AND METHODS” and “RESULTS”. After using this tool/service, the author(s) reviewed and edited the content as needed and take(s) full responsibility for the content of the publication.

BIBLIOGRAPHY

1. Anderson NM, Simon MC. The tumor microenvironment. *Curr Biol*. 2020;30(16):R921-R925. doi:10.1016/J.CUB.2020.06.081

2. Semeniuk-Wojtaś A, Poddębniak-Strama K, Modzelewska M, et al. Tumour microenvironment as a predictive factor for immunotherapy in non-muscle-invasive bladder cancer. *Cancer Immunol Immunother*. 2023;72(7):1971-1989. doi:10.1007/S00262-023-03376-9

3. Ma Z, Li X, Mao Y, et al. Interferon-dependent SLC14A1+ cancer-associated fibroblasts promote cancer stemness via WNT5A in bladder cancer. *Cancer Cell*. 2022;40(12):1550-1565.e7. doi:10.1016/J.CCELL.2022.11.005

524 4. Lee YC, Lam HM, Rosser C, Theodorescu D, Parks WC, Chan KS. The dynamic
525 roles of the bladder tumour microenvironment. *Nat Rev Urol*. 2022;19(9):515-
526 533. doi:10.1038/S41585-022-00608-Y

527 5. Chen Z, Zhou L, Liu L, et al. Single-cell RNA sequencing highlights the role of
528 inflammatory cancer-associated fibroblasts in bladder urothelial carcinoma. *Nat*
529 *Commun*. 2020;11(1). doi:10.1038/S41467-020-18916-5

530 6. Mariathasan S, Turley SJ, Nickles D, et al. TGFβ attenuates tumour response to
531 PD-L1 blockade by contributing to exclusion of T cells. *Nature*.
532 2018;554(7693):544-548. doi:10.1038/NATURE25501

533 7. Gómez del Cañizo C, Rodríguez-Izquierdo Jiménez M, Peña Vallejo E, et al. New
534 immunotherapies for high-risk non-muscle invasive bladder cancer: Current
535 state and future perspectives. *Actas Urol Esp*. 2020;44(9):574-585.
536 doi:10.1016/J.ACURO.2020.06.011

537 8. Kamat AM, Hahn NM, Efstathiou JA, et al. Bladder cancer. *Lancet (London,*
538 *England)*. 2016;388(10061):2796-2810. doi:10.1016/S0140-6736(16)30512-8

539 9. Balar A V., Kamat AM, Kulkarni GS, et al. Pembrolizumab monotherapy for the
540 treatment of high-risk non-muscle-invasive bladder cancer unresponsive to BCG
541 (KEYNOTE-057): an open-label, single-arm, multicentre, phase 2 study. *Lancet*
542 *Oncol*. 2021;22(7):919-930. doi:10.1016/S1470-2045(21)00147-9

543 10. Black PC, Tangen C, Singh P, et al. Phase II trial of atezolizumab in BCG-
544 unresponsive non-muscle invasive bladder cancer: SWOG S1605 (NCT
545 #02844816). *https://doi.org/101200/JCO20213915_suppl4541*.

546 2021;39(15_suppl):4541-4541. doi:10.1200/JCO.2021.39.15_SUPPL.4541

547 11. Martínez VG, Rubio C, Martínez-Fernández M, et al. BMP4 Induces M2
548 Macrophage Polarization and Favors Tumor Progression in Bladder Cancer. *Clin*
549 *Cancer Res*. 2017;23(23):7388-7399. doi:10.1158/1078-0432.CCR-17-1004

550 12. de Villarreal JM, Kalisz M, Piedrafita G, et al. Pseudoalignment tools as an
551 efficient alternative to detect repeated transposable elements in scRNAseq
552 data. *Bioinformatics*. 2023;39(1). doi:10.1093/BIOINFORMATICS/BTAC737

553 13. DeTomaso D, Jones MG, Subramaniam M, Ashuach T, Ye CJ, Yosef N. Functional
554 interpretation of single cell similarity maps. *Nat Commun*. 2019;10(1).
555 doi:10.1038/S41467-019-12235-0

556 14. Rimm DL, Camp RL, Charette LA, Olsen DA, Provost E. Amplification of tissue by
557 construction of tissue microarrays. *Exp Mol Pathol*. 2001;70(3):255-264.
558 doi:10.1006/exmp.2001.2363

559 15. Ma RY, Black A, Qian BZ. Macrophage diversity in cancer revisited in the era of
560 single-cell omics. *Trends Immunol*. 2022;43(7):546-563.
561 doi:10.1016/J.IT.2022.04.008

562 16. Lindskrog SV, Prip F, Lamy P, et al. An integrated multi-omics analysis identifies
563 prognostic molecular subtypes of non-muscle-invasive bladder cancer. *Nat*
564 *Commun*. 2021;12(1). doi:10.1038/S41467-021-22465-W

565 17. Sun X, Xu H, Liu G, et al. A Robust Immuno-Prognostic Model of Non-Muscle-
566 Invasive Bladder Cancer Indicates Dynamic Interaction in Tumor Immune
567 Microenvironment Contributes to Cancer Progression. *Front Genet*. 2022;13.

568 doi:10.3389/FGENE.2022.833989

569 18. Damrauer JS, Roell KR, Smith MA, et al. Identification of a Novel Inflamed Tumor
570 Microenvironment Signature as a Predictive Biomarker of Bacillus Calmette-
571 Guérin Immunotherapy in Non-Muscle-Invasive Bladder Cancer. *Clin Cancer Res*.
572 2021;27(16):4599-4609. doi:10.1158/1078-0432.CCR-21-0205

573 19. Robertson AG, Groeneveld CS, Jordan B, et al. Identification of Differential
574 Tumor Subtypes of T1 Bladder Cancer. *Eur Urol*. 2020;78(4):533-537.
575 doi:10.1016/J.EURURO.2020.06.048

576 20. Zheng Z, Mao S, Zhang W, et al. Dysregulation of the Immune Microenvironment
577 Contributes to Malignant Progression and Has Prognostic Value in Bladder
578 Cancer. *Front Oncol*. 2020;10. doi:10.3389/FONC.2020.542492

579 21. Martínez R, Tapia G, De Muga S, et al. Combined assessment of peritumoral
580 Th1/Th2 polarization and peripheral immunity as a new biomarker in the
581 prediction of BCG response in patients with high-risk NMIBC. *Oncoimmunology*.
582 2019;8(8). doi:10.1080/2162402X.2019.1602460

583 22. Pichler R, Fritz J, Zavadil C, Schäfer G, Culig Z, Brunner A. Tumor-infiltrating
584 immune cell subpopulations influence the oncologic outcome after intravesical
585 Bacillus Calmette-Guérin therapy in bladder cancer. *Oncotarget*.
586 2016;7(26):39916-39930. doi:10.18632/ONCOTARGET.9537

587 23. Nunez-Nateras R, Castle EP, Protheroe CA, et al. Predicting response to bacillus
588 Calmette-Guérin (BCG) in patients with carcinoma in situ of the bladder. *Urol*
589 *Oncol*. 2014;32(1):45.e23-45.e30. doi:10.1016/J.UROLONC.2013.06.008

590 24. Hanada T, Nakagawa M, Emoto A, Nomura T, Nasu N, Nomura Y. Prognostic
591 value of tumor-associated macrophage count in human bladder cancer. *Int J*
592 *Urol*. 2000;7(7):263-269. doi:10.1046/J.1442-2042.2000.00190.X

593 25. Miyake M, Tatsumi Y, Gotoh D, et al. Regulatory T Cells and Tumor-Associated
594 Macrophages in the Tumor Microenvironment in Non-Muscle Invasive Bladder
595 Cancer Treated with Intravesical Bacille Calmette-Guérin: A Long-Term Follow-
596 Up Study of a Japanese Cohort. *Int J Mol Sci*. 2017;18(10).
597 doi:10.3390/IJMS18102186

598 26. Suriano F, Santini D, Perrone G, et al. Tumor associated macrophages
599 polarization dictates the efficacy of BCG instillation in non-muscle invasive
600 urothelial bladder cancer. *J Exp Clin Cancer Res*. 2013;32(1). doi:10.1186/1756-
601 9966-32-87

602 27. Blinova E, Buzdin A, Enikeev D, et al. Prognostic Role of FGFR3 Expression Status
603 and Tumor-Related MicroRNAs Level in Association with PD-L1 Expression in
604 Primary Luminal Non-Muscular Invasive Bladder Carcinoma. *Life (Basel,*
605 *Switzerland)*. 2020;10(11):1-14. doi:10.3390/LIFE10110305

606 28. Viveiros N, Flores BCT, Lobo J, et al. Detailed bladder cancer immunoprofiling
607 reveals new clues for immunotherapeutic strategies. *Clin Transl Immunol*.
608 2022;11(9). doi:10.1002/CTI2.1402

609 29. Kubon J, Sikic D, Eckstein M, et al. Analysis of CXCL9, PD1 and PD-L1 mRNA in
610 Stage T1 Non-Muscle Invasive Bladder Cancer and Their Association with
611 Prognosis. *Cancers (Basel)*. 2020;12(10):1-13. doi:10.3390/CANCERS12102794

612 30. Breyer J, Wirtz RM, Otto W, et al. High PDL1 mRNA expression predicts better
613 survival of stage pT1 non-muscle-invasive bladder cancer (NMIBC) patients.
614 *Cancer Immunol Immunother*. 2018;67(3):403-412. doi:10.1007/S00262-017-
615 2093-9

616 31. Eich ML, Chaux A, Guner G, et al. Tumor immune microenvironment in non-
617 muscle-invasive urothelial carcinoma of the bladder. *Hum Pathol*. 2019;89:24-
618 32. doi:10.1016/J.HUMPATH.2019.04.003

619 32. Roumiguié M, Compérat E, Chaltiel L, et al. PD-L1 expression and pattern of
620 immune cells in pre-treatment specimens are associated with disease-free
621 survival for HR-NMIBC undergoing BCG treatment. *World J Urol*.
622 2021;39(11):4055-4065. doi:10.1007/S00345-020-03329-2

623 33. Wankowicz SAM, Werner L, Orsola A, et al. Differential Expression of PD-L1 in
624 High Grade T1 vs Muscle Invasive Bladder Carcinoma and its Prognostic
625 Implications. *J Urol*. 2017;198(4):817-823. doi:10.1016/J.JURO.2017.04.102

626 34. Aydin AM, Baydar DE, Hazir B, Babaoglu B, Bilen CY. Prognostic significance of
627 pre- and post-treatment PD-L1 expression in patients with primary high-grade
628 non-muscle-invasive bladder cancer treated with BCG immunotherapy. *World J*
629 *Urol*. 2020;38(10):2537-2545. doi:10.1007/S00345-019-03065-2

630 35. Tretiakova M, Fulton R, Kocherginsky M, et al. Concordance study of PD-L1
631 expression in primary and metastatic bladder carcinomas: comparison of four
632 commonly used antibodies and RNA expression. *Mod Pathol*. 2018;31(4):623-
633 632. doi:10.1038/MODPATHOL.2017.188

634 36. Cha JH, Chan LC, Li CW, Hsu JL, Hung MC. Mechanisms Controlling PD-L1
635 Expression in Cancer. *Mol Cell*. 2019;76(3):359-370.
636 doi:10.1016/J.MOLCEL.2019.09.030

637 37. Caramelo B, Zagorac S, Corral S, Marqués M, Real FX. Cancer-associated
638 Fibroblasts in Bladder Cancer: Origin, Biology, and Therapeutic Opportunities.
639 *Eur Urol Oncol*. 2023;6(4):366-375. doi:10.1016/J.EUO.2023.02.011

640 38. Shin K, Lim A, Zhao C, et al. Hedgehog signaling restrains bladder cancer
641 progression by eliciting stromal production of urothelial differentiation factors.
642 *Cancer Cell*. 2014;26(4):521-533. doi:10.1016/J.CCELL.2014.09.001

643 39. Du YH, Sui YQ, Cao J, et al. Dynamic Changes in Myofibroblasts Affect the
644 Carcinogenesis and Prognosis of Bladder Cancer Associated With Tumor
645 Microenvironment Remodeling. *Front cell Dev Biol*. 2022;10.
646 doi:10.3389/FCELL.2022.833578

647 40. Li B, Pei G, Yao J, Ding Q, Jia P, Zhao Z. Cell-type deconvolution analysis identifies
648 cancer-associated myofibroblast component as a poor prognostic factor in
649 multiple cancer types. *Oncogene*. 2021;40(28):4686-4694. doi:10.1038/S41388-
650 021-01870-X

651 41. Mezheyeuski A, Segersten U, Leiss LW, et al. Fibroblasts in urothelial bladder
652 cancer define stroma phenotypes that are associated with clinical outcome. *Sci*
653 *Rep*. 2020;10(1). doi:10.1038/S41598-019-55013-0

654 42. Miyake M, Hori S, Morizawa Y, et al. CXCL1-Mediated Interaction of Cancer Cells
655 with Tumor-Associated Macrophages and Cancer-Associated Fibroblasts

656 Promotes Tumor Progression in Human Bladder Cancer. *Neoplasia*.
657 2016;18(10):636-646. doi:10.1016/J.NEO.2016.08.002

658 43. Grimm S, Jennek S, Singh R, et al. Malignancy of bladder cancer cells is enhanced
659 by tumor-associated fibroblasts through a multifaceted cytokine-chemokine
660 loop. *Exp Cell Res*. 2015;335(1):1-11. doi:10.1016/J.YEXCR.2015.04.001

661 44. Wang P, Nishitani MA, Tanimoto S, et al. Bladder cancer cell invasion is
662 enhanced by cross-talk with fibroblasts through hepatocyte growth factor.
663 *Urology*. 2007;69(4):780-784. doi:10.1016/J.UROLOGY.2007.01.063

664 45. Lo A, Wang LCS, Scholler J, et al. Tumor-Promoting Desmoplasia Is Disrupted by
665 Depleting FAP-Expressing Stromal Cells. *Cancer Res*. 2015;75(14):2800-2810.
666 doi:10.1158/0008-5472.CAN-14-3041

667 46. Koivisto MK, Tervahartiala M, Kenessey I, Jalkanen S, Boström PJ, Salmi M. Cell-
668 type-specific CD73 expression is an independent prognostic factor in bladder
669 cancer. *Carcinogenesis*. 2019;40(1):84-92. doi:10.1093/CARCIN/BGY154

670 47. Benjamin DJ, Lyou Y. Advances in Immunotherapy and the TGF-β Resistance
671 Pathway in Metastatic Bladder Cancer. *Cancers (Basel)*. 2021;13(22).
672 doi:10.3390/CANCERS13225724

673 48. Liu Z, Qi T, Li X, et al. A Novel TGF-β Risk Score Predicts the Clinical Outcomes
674 and Tumour Microenvironment Phenotypes in Bladder Cancer. *Front Immunol*.
675 2021;12. doi:10.3389/FIMMU.2021.791924

676 49. Zhuang J, Lu Q, Shen B, et al. TGFβ1 secreted by cancer-associated fibroblasts
677 induces epithelial-mesenchymal transition of bladder cancer cells through

678 lncRNA-ZEB2NAT. *Sci Rep*. 2015;5. doi:10.1038/SREP11924

679 50. Biffi G, Tuveson DA. Diversity and Biology of Cancer-Associated Fibroblasts.

680 *Physiol Rev*. 2021;101(1):147-176. doi:10.1152/PHYSREV.00048.2019

681